Supporting Information for:

Unraveling the Primary Isomerization Dynamics in Cyanobacterial Phytochrome Cph1 with Multipulse Manipulations

Peter W. Kim,[1] Nathan C. Rockwell,[2] Lucy H. Freer,[1] Che-Wei Chang,[1] Shelley S. Martin,[2] J. Clark Lagarias,[2] and Delmar S. Larsen[1]*

[1]*Department of Chemistry, University of California, One Shields Avenue, Davis, CA 95616*

[2]*Department of Molecular and Cell Biology, University of California, One Shields Avenue, Davis, CA 95616*

*Corresponding Author: dlarsen@ucdavis.edu

S1. Ultrafast Pump-Dump-Probe (PDP) Experimental Set-up

The primary ultrafast laser source was an amplified Ti:sapphire laser system (Spectra Physics Spitfire Pro) that delivered 800-nm pulses with a 2.3-mJ pulse energy at a 1-kHz repetition rate and 40-fs full width at half maximum (FWHM) pulse duration. The laser output was split into three separate pathways for generating pump, dump and probe pulses. The broadband white light probe pulses were generated by focusing the 800-nm pulses into a slowly translating 2-mm CaF_2 crystal. The generated probe light was then focused onto the sample and dispersed by commercial spectrograph (Oriel MS125) to be detected with a linear 256-pixel photodiode array (Hamamatsu S3901 and C7884).

The pump and dump pulses were generated by home-built non-collinear optical parametric amplifiers (NOPA) that produced tunable visible excitation and de-excitation pulses.[1] The pump pulses had a 615-nm central wavelength with 30-nm FWHM bandwidth and 300-nJ pulse energy. A second independent two-stage NOPA was used to generate the 725-nm dump pulses. The first stage involved a NOPA that generated a seed beam that was filtered (λ_{center} = 725 nm, 7-nm bandwidth) and amplified by a second NOPA. This amplified light was filtered again by another interference filter (λ_{center} = 725 nm, $\Delta\lambda$ = 7 nm). An instrument response function (IRF) of 150 fs was estimated by the rise time of excited-state absorption (ESA) band of the pump-probe signals of IR-140 laser dye with the 725-nm light as the pump source and broadband white light as a probe showed. The energy of the dump pulses was 900 nJ/pulse at the sample.

The pump beam was chopped at 500 Hz to generate difference spectra with respect to the non-pumped probe spectrum. The dump beam was chopped at 250 Hz to generate pump-dump-probe pulse sequence. The probe beam was optically delayed with respect to the pump pulse with a computer controlled linear-motor stage (Newport IMS600LM), which allowed up to 7-ns temporal separation. The dump beam was also delayed 2.3 and 10 ps after the pumping to generate two independent PDP datasets (collected on different days). The pump and dump pulses were linearly polarized (parallel) to each other and set to 54.7^o (magic angle) with respect to probe pulse polarization. Pump and dump pulse spot diameters of 250 to 360 μm were estimated using a micrometer stage and razor blade; the broadband probe pulses were focused to ~50 μm. The appreciably greater pump pulse volume minimizes artifactual contributions to the signals due to varying spatial overlap between pump and probe beams. This minimization was confirmed by monitoring signal amplitude and spectral shape while dithering the pump beam with respect to the probe beam.

The temporal resolution of the PP and DP signals were estimated at 100 fs and 150 fs using the rise time of the excited-state absorption bands. The sample was flowed continuously in a closed circuit to ensure fresh sample for each excitation pulse. Before the sample entered the cuvette, it was illuminated with a far-red light emitting diode (Epitex inc., L720-66-60) through a quartz window to maintain the desired P_r photostate. The path length of the quartz cuvette was 2 mm,

and the optical density at the red absorbance band was 0.4-0.5 at that path length. All experiments were performed at room temperature.

S2. Lumi-R Depletion

In any double resonant experiment, there exists the potential for multiple transitions to be "pumped" by the second applied pulse, which can result in complicated data analysis and interpretation.[2-3] In an ideal PDP experiment, the dump will only be resonant with the SE band ($S_1 \rightarrow S_0$) and demote a portion of the excited-state population back to the ground-state surface. However, the dump pulse can also trigger four other transitions in Cph1: (1) pumping the ground-state P_r population ($P_r \rightarrow P_r^*$), (2) pumping the metastable P_{fr} population ($P_{fr} \rightarrow P_{fr}^*$) formed by previous photoexcitations, (3) pumping of the primary Lumi-R photoproduct ($S_0 \rightarrow S_1$), and (4) repumping the excited-state P_r^* population ($S_1 \rightarrow S_n$):

1. The first possibility of pumping the P_r population can be easily excluded from our analysis, as there is negligible spectral overlap of the dump laser spectrum with the P_r ground-state spectra (Figure 2A). This is further supported by the lack of photoexcited P_r pump-probe signals in the DP channel (Figure S2) of the PDP datasets.
2. The second possibility of exciting P_{fr} **was** observed in our signals (although weakly) whereby the dump pulse initiated Cph1 reverse dynamics (Figure S2).[4] Since this is a separate and independent signal than the PP (and PDP) signals, arising from different pump populations, it can be simply subtracted from PDP signals (i.e., PDP-DP) without adversely affecting the analysis and interpretation. The DP signals are near-zero (< 0.5 mOD) in less than 1 ps after the application of the dump pulse (Figure S2) and have very different spectral and kinetic properties than the P_r^* initiated signals.[4]
3. The third possibility of exciting Lumi-R can be excluded since no spectral overlap exists between Lumi-R and the dump spectrum (Figure 2, magenta curve).
4. Excluding the fourth possibility of repumping of P_r^* into one or more higher-lying states[5-6] requires more discussion. Repumping P_r^* may decrease the Lumi-R product yield by initiating higher-energy photochemistry (e.g., ionization, isomerization, or dissociation) separate from the isomerization reaction on the lower excited-state energy surface.[5, 7] For this mechanism to be efficient, the 725-nm dump pulse *must* be resonant with an ESA ($S_1 \rightarrow S_n$); this is inconsistent with the PP signals (Figure 2B), which exhibit no clearly resolved (positive) ESA at the 725-nm dump wavelength and only exhibit a strong negative SE band in the visible broadband spectral window. Hence, if a repumped P_r^* signal were to existed, it would result from repumping a hidden ESA band that is far obscured by the SE band. Thus repumping of P_r^* is likely a minor contributor to PDP signals (see below for discussion).

The near-infrared (NIR) pump-probe signals (765 to 815 nm) indicate that the negative SE signals extend to 780 nm (Figure S3A) and persist to 50 ps. There is an ESA band overlapping with SE band, however, as evidenced from the 790-nm probe (Figure S3B), which shows the negative signal being quickly overtaken by the ESA signals. Moreover, the SE in this region

undergoes apparent "blue-shifting" (Figure S4) as it decays while ESA persists. The SE and ESA bands show clearly distinct kinetics, with the SE band exhibiting faster excited-state decay kinetics than the ESA signals (Figure S3A vs. S3D, respectively). This is ascribed to the heterogeneity of P_r, with the slowly decaying ESA band attributed to the fluorescent subpopulations.[8] At 10 ps, this slow NIR ESA band predominates at wavelengths further red than the 780-nm region (Figure S4, red curve), but the SE band is stronger at 725 nm and therefore $S_1 \rightarrow S_n$ repumping transitions caused by the 725-nm dump pulse are expected to minimal compared to $S_1 \rightarrow S_0$ dumping.

Furthermore, the P_r* population is depleted by the dump pulse by ~25 % and ~20 % for the 10-ps and 2.3-ps dump data, respectively, and is maintained at that level up to 120 ps (Figure S5). Assuming that a hidden higher lying excited-state population is further excited by the 725-nm dump pulse, the S_1 state would be at least partially repopulated as the repumped population trickles down the excited-state manifold.[6] For 10-ps dump induced P_r* percent change, a small increase (~ 10 % of the percent change) is observed in first 2 ps after the application of the dump pulse (Figure S5A); 2.3-ps dump-induced percent change does not show such increase (Figure S5B). Within S/N of PDP signals, the small increase observed in 10-ps P_r* percent change is insufficient to support P_r* repumping mechanism. Hence, the observed P_r* (and Lumi-R) depletion is mostly (> 90 %) attributed to the dumping ($S_1 \rightarrow S_0$) of the excited-state P_r* population. In the integrated model (Figure S12A and S14A), given limited S/N of PDP signals (Figure S9 and S11) and likely a minor contribution of P_r* repumping in PDP signals, P_r* repumping mechanism was not considered, which resulted in self-consistent model (see below for further discussion) to describe the 2.3-ps, 10-ps PDP signals in this study and the temperature-dependent PP studies.[8]

S3. Global Analysis

Instead of analyzing individual kinetic traces, the multi-wavelength signals were analyzed within a global analysis formalism[9-10] that fits the data to an underlying postulated multi-population "target" model and estimates the concentration profiles and spectra of the constituent populations. This is accomplished by fitting the data with numerical solutions of linear first-order differential equations describing a postulated model (Eq. 1):

$$\frac{dn_i}{dt} = A_i I_{pump}(t) + \sum_j [K_{ij} + C_{ij} I_{dump}(t)] n_j \qquad \text{Equation (1)}$$

In Equation 1, n_i represents the i^{th} microscopic population, while $I_{pump}(t)$ and $I_{dump}(t)$ represent the pump and dump pulse temporal envelopes, respectively. A_i is the initial occupancy of excited population for i^{th} microscopic population and C_{ij} is the populations that are dumped. K_{ij} is the rate constant matrix describing the *exponential* flow from one population into another. If the underlying target model accurately describes the dynamics, the extracted spectra for the populations are Species-Associated-Difference-Spectra (SADS) and represent the true difference spectra of the constituent populations. If the model is inaccurate, the resulting spectra are

Evolutionary-Associated-Difference-Spectra (EADS) and are combinations of the underlying SADS, but such EADS can still be used as a basis for describing the data.[9-10] The integrated solutions to the linear differential equations in Eq. 1 are an ensemble of single exponentials, which is appropriate for first-order processes. The details of global analysis of Cph1's forward reaction dynamics and its target model for temperature and excitation-dependent PP transient spectra are presented elsewhere,[8] which is the basis of the analysis in this manuscript.

S3.1 Sequential Analysis of PP Signals to Characterize Excited-State Dynamics

The PP signals were first analyzed by a sequential global analysis and the model with 6 components was chosen (Figure S6A). This is consistent with the temperature-dependent PP studies,[8] and this allows good characterization of the slower fluorescent population with 1.3-ns lifetime component. The PP signals from both 10-ps and 2.3-ps dump datasets had comparable results, and only the 10-ps dumped data set is presented here (Figure S6). The fit to the data is excellent (Figure S7) and resolves complex multi-exponential excited-state decay dynamics, including Lumi-R formation. The kinetic components and time constants closely reproduced those from the recent temperature and excitation-dependent PP signals,[8] with small spectral deviations that could arise from sample variations or slight variations in pulse width, sample temperature, or other experimental conditions.

The EADS estimated from the sequential analysis (Figure S6B) were normalized at the ESA band of the 440 to 500 nm region (Figure S6C), which contains excited-state signals with minimal bleach contribution. These normalized EADS were subtracted in sequence (i.e., normalized EADS2 – normalized EADS1, normalized EADS3 – normalized EADS2, etc.) to separate spectral evolution from excited-state population decay. Figure S6D shows the difference between normalized EADS4 and EADS3 (green curve), and EADS5 and EADS4 (purple curve). The difference between the normalized EAD4 and EADS3 originates from the difference between the SADS of the faster-decaying photoactive subpopulations and the slowly-decaying fluorescent subpopulations.[8] The difference between normalized EADS5 and EADS4 is attributed to Lumi-R formation (i.e., PP EADS6).

S3.2 Sequential analysis of ΔΔOD Signals to Characterize Ground-state Evolution

For the PDP signals, we first analyzed the ΔΔOD (PDP – PP – DP) signals with a sequential model like the PP signals discussed above (Figure S8A and S10A). The ΔΔOD signals track the dump-induced changes to the PP signals and allow for the exclusive examination of the dumping effects without having to simultaneously model the PP and PDP signals. For the 10-ps dump data, a sequential three-components model was used (Figure S8A, inset) to extract decay time constants of 14 ps, 165 ps, and a non-decaying ($\tau = \infty$) component. Due to low S/N of ΔΔOD signals, all of the excited-state decay constants associated with PP signal analysis (Figure S6A) could not be resolved, although the general fit to the data was good (Figure S9). For the 2.3-ps dump data, also a three-component sequential model was needed with 12 ps, 204 ps and a non-

decaying ($\tau = \infty$) component (Figure S10A). These decay components are comparable to those obtained for the 10-ps dump data.

If the dump pulse exclusively de-excites a portion of the excited-state population to its original P_r ground-state, the ΔΔOD signal will be an inversion of the PP spectra and will track the post-dumping PP dynamics. However, the dump pulse could generate a distinct ground-state species (i.e., a ground-state intermediate or GSI), whose spectral and temporal signature in the ΔΔOD signals would appear as a deviation from the PP (depletion) signals.[11] To extract potential GSI dynamics in Cph1 PDP signals, the ΔΔOD signals were contrasted to the PP signals (Figure S8 and S10 for 10-ps and 2.3-ps PDP data, respectively). The ΔΔOD signals are scaled to the ESA band from 440 to 500 nm. For the 10-ps dump data set, ΔΔOD EADS1 was compared with PP EADS3, which was selected due to its relevance at the 10 ps probe time (Figure S8C, black and dark cyan curves, respectively), and they show comparable spectral shape except in 575 to 675 nm region. The difference between ΔΔOD EADS1 and PP EADS3 (Figure S8C, orange curve) looks comparable to P_r ground state absorption band with possible loss of Lumi-R contribution from PP EADS3. However, poor S/N of raw data (Figure S9) does not allow clear identification of GSI populations here. For the 2.3-ps PDP data set, ΔΔOD EADS1 was compared with PP EADS2 (PP EADS1 and EADS2 are similar to each other, Figure S6C) with the very similar result to 10-ps dump signals (Figure S10C). Again due to poor S/N of raw data (Figure S11), a conclusive identification of GSI was not reasonable. Therefore, GSI population was not included in the integrated model to describe both 10-ps and 2.3-ps dump data (Figure S12A and S14A, respectively), although our data and analysis does not conclusively rule out the presence of GSI populations suggested by van Thor and co-workers.[2-3]

The ΔΔOD EADS2 for both 10-ps and 2.3-ps are compared with SADS of the fluorescent population from the integrated model (Figure S8D and S10D, respectively), showing good overlap. This indicates the dump pulse effectively de-exciting both photoactive and fluorescent populations deduced from the temperature-dependent PP signals.[8]

S3.3 Simultaneous Target Analysis of PDP (PP, PDP, and ΔΔOD) Signals

A more complete target analysis was applied to simultaneously fit the PDP datasets (including PP, PDP, and ΔΔOD signals) to extract the microscopic rate constants that describe one microscopic population evolving into another. Using the previously constructed inhomogeneous model,[8] combined with the PP and ΔΔOD sequential analyses above (Figures S6 for PP, S8 and S10 for 10-ps and 2.3-ps PDP data set ΔΔOD analysis, respectively), the target model was constructed by fitting both 10-ps and 2.3-ps PDP datasets (Figures S12A and S14A, respectively). Listed below are the spectral and *a priori* constraints used in constructing the target model:

1. The multi-exponential excited-state dynamics originated from heterogeneous populations[8]: photoactive subpopulations with faster excited-state kinetics that generate Lumi-R, and fluorescent subpopulations with slower excited-state kinetics

(analogous to Cph1 Y176H fluorophore[12]). Both subpopulations have distinct spectral and kinetic properties, although the ESA band from 440 to 500 nm is expected to be spectrally similar for each. Dump pulse induced depletion of both populations.

2. The dump pulse efficiency of Lumi-R depletion is dump-time dependent (Figure S17), where the efficiency (Lumi-R depletion/P_r* depletion x 100 %) was ~40 % and ~80 % for the 10-ps and 2.3-ps dump PDP data, respectively.
3. GSI population is not included in the model as discussed above.

The respective target models (10-ps and 2.3-ps PDP data for Figure S12A and S14A, respectively) have a total of five subpopulations, with two belonging to photoactive populations (P_r 1 and 2) and three others to fluorescent populations (P_r 3 and 5). Only P_r 2 generates Lumi-R photoproduct in agreement with the PP sequential analysis (Figure S6D) that indicates Lumi-R photoproduct is also being generated in later times (> 100 ps). For both 10-ps and 2.3-ps PDP datasets, the connectivity and time constants are identical to the 25 °C model from temperature-dependent study.[8] However, the occupation of each population in the signals (indicated in the box of the respective subpopulations) varies (e.g., the occupation of P_r 1 is 29 % and 16 % for 10-ps and 2.3-ps PDP data). This is likely due to sample-to-sample and experimental condition variations, as temperature and excitation-dependent PP studies demonstrated that Cph1's initial dynamics are very sensitive to such conditions.[8]

The goodness of fit is shown at selected wavelengths (Figure S13 and S15 for 10-ps and 2.3-ps PDP data). In order to adequately fit the PDP traces without adding GSI population, dump efficiency of 30 % and 25 % was applied for 10-ps and 2.3-ps dump data. This is somewhat higher than dump efficiency estimated by overall ESA depletion percentage at 25 % and 20 % for 10-ps and 2.3-ps dump data (Figure S5). The dump efficiency between the photoactive and fluorescent subpopulations may be different. Or the coherent artifact between dump and probe beams makes the initial depletion magnitude greater than actual P_r* depletion. In this study, all subpopulations were assumed to have same depletion efficiency and its magnitude was adjusted for the best fit.

The extracted SADS of 10-ps and 2.3-ps PDP and 25 °C temperature-dependent PP studies are compared side-by-side (Figure S16) showing good overlap, especially between 10-ps and 2.3-ps PDP signals. Slight deviation of the temperature-dependent SADS is likely due to excitation-wavelength dependence on the excited-state spectra that was observed in excitation-wavelength dependence study.[8, 13] The good consistency between signals from independent experiments helps validate the integrated model proposed here (Figure S12A and S14A).

The model predicts Lumi-R quantum yield for the 10-ps and 2.3-ps PP datasets at 12.3 % and 15.5 %, respectively, and for PDP at 10.4 % and 12.5 % (Figure S12C and 14C) with P_r* depletion modeled at 30 % and 25 %, respectively. This gives a relative Lumi-R depletion ([% Lumi-R depletion]/[% P_r*] x 100 %) of 51 % and 77 %, respectively. The dump time dependence in relative Lumi-R depletion is due to more Lumi-R already generated at 10 ps

compared to at 2.3 ps, given that pump pulse only affects P_r* population as discussed above. This Lumi-R depletion was further explored by independent measurement (albeit with the same sample, excitation and de-excitation conditions) with high average counts (Figure 5 for 10-ps dump signals) to improve S/N of dump-induced initial excited-state populations and Lumi-R depletion (ΔΔOD/PP x 100 %, Figure S17). For the 10-ps PDP data, the excited-state population was de-excited by ~25 % and Lumi-R was depleted ~10 %, which gives 40 % Lumi-R depletion. For the 2.3-ps PDP data, the initial excited-state dump efficiency was 22 % and Lumi-R was 17 %, to produce a relative Lumi-R depletion of 78 %. The 2.3-ps PDP data show excellent agreement between two methods.

For the 10-ps PDP signals, slight discrepancy (51 % vs. 40 %) exists between two methods. For the high-average PDP signals (Figure 5), the initial P_r* depletion was estimated at 11 ps, which is 1 ps after the dump pulse. In contrast 2.3-ps PDP signals' initial P_r* depletion was estimated at 3 ps, 700 fs after. Due to a small initial decrease of the % depletion (Figure S5), the 10-ps high-average PDP might have underestimated P_r* depletion more. Also at 10 ps, due to lower magnitude of P_r* signals in comparison to the signals at 2.3 ps (Figure S7), the S/N is more poor to make accurate estimations more difficult. However, this minor error does not affect interpretations of PDP signals presented here.

References

(1) Cerullo, G.; Nisoli, M.; Stagira, S.; De Silvestri, S. Sub-8-fs Pulses from an Ultrabroadband Optical Parametric Amplifier in the Visible. *Opt. Lett.* **1998,** *23*, 1283-1285.

(2) Fitzpatrick, A. E.; Lincoln, C. N.; van Wilderen, L. J.; van Thor, J. J. Pump-Dump-Probe and Pump-Repump-Probe Ultrafast Spectroscopy Resolves Cross Section of an Early Ground State Intermediate and Stimulated Emission in the Photoreactions of the Pr Ground State of the Cyanobacterial Phytochrome Cph1. *J. Phys. Chem. B* **2012,** *116*, 1077-88.

(3) van Wilderen, L.; Clark, I. P.; Towrie, M.; van Thor, J. J. Mid-Infrared Picosecond Pump-Dump-Probe and Pump-Repump-Probe Experiments to Resolve a Ground-State Intermediate in Cyanobacterial Phytochrome Cph1. *J. Phys. Chem. B* **2009,** *113*, 16354-16364.

(4) Kim, P. W.; Pan, J.; Rockwell, N. C.; Chang, C.-W.; Taylor, K. C.; Lagarias, J. C.; Larsen, D. S. Ultrafast E to Z Photoisomerization Dynamics of the Cph1 Phytochrome. *Chem. Phys. Lett.* **2012,** *549*, 86-92.

(5) Larsen, D. S.; Vengris, M.; van Stokkum, I. H. M.; van der Horst, M. A.; de Weerd, F. L.; Hellingwerf, K. J.; van Grondelle, R. Photoisomerization and Photoionization of the Photoactive Yellow Protein Chromophore in Solution. *Biophys. J.* **2004,** *86*, 2538-2550.

(6) Larsen, D. S.; Papagiannakis, E.; van Stokkum, I. H. M.; Vengris, M.; Kennis, J. T. M.; van Grondelle, R. Excited State Dynamics of Beta-carotene Explored with Dispersed Multi-pulse Transient Absorption. *Chem. Phys. Lett.* **2003,** *381*, 733-742.

(7) Larsen, D. S.; van Stokkum, I. H. M.; Vengris, M.; van der Horst, M. A.; de Weerd, F. L.; Hellingwerf, K. J.; van Grondelle, R. Incoherent Manipulation of the Photoactive Yellow Protein Photocycle with Dispersed Pump-dump-probe Spectroscopy. *Biophys. J.* **2004,** *87*, 1858-1872.

(8) Kim, P. W.; Rockwell, N. C.; Martin, S. S.; Lagarias, J., Clark; Larsen, D. S. Dynamic Inhomogeneity in the Cyanobacterial Phytochrome Cph1, In preparation.

(9) van Stokkum, I. H. M.; Larsen, D. S.; van Grondelle, R. Global and Target Analysis of Time-resolved Spectra. *BBA-Bioenergetics* **2004,** *1657*, 82-104.
(10) Holzwarth, A. R. *Biophysical Techniques in Photosynthesis*; Springer: Netherlands, 1996.
(11) Kim, P. W.; Freer, L. H.; Rockwell, N. C.; Martin, S. S.; Lagarias, J. C.; Larsen, D. S. Second-Chance Forward Isomerization Dynamics of the Red/Green Cyanobacteriochrome NpR6012g4 from Nostoc punctiforme. *J. Am. Chem. Soc.* **2012,** *134*, 130-133.
(12) Fischer, A. J.; Lagarias, J. C. Harnessing Phytochrome's Glowing Potential. *Proc. Natl. Acad. Sci.* **2004,** *101*, 17334-17339.
(13) Demchenko, A. P. The Red-Edge Effects: 30 years of Exploration. *Luminescence* **2002,** *17*, 19-42.
(14) Dasgupta, J.; Frontiera, R. R.; Taylor, K. C.; Lagarias, J. C.; Mathies, R. A. Ultrafast Excited-State Isomerization in Phytochrome Revealed by Femtosecond Stimulated Raman Spectroscopy. *Proc. Natl. Acad. Sci.* **2009,** *106*, 1784-1789.
(15) Lamparter, T.; Mittmann, F.; Gartner, W.; Borner, T.; Hartmann, E.; Hughes, J. Characterization of Recombinant Phytochrome from the Cyanobacterium Synechocystis. *Proc. Natl. Acad. Sci.* **1997,** *94*, 11792-11797.

Figures:

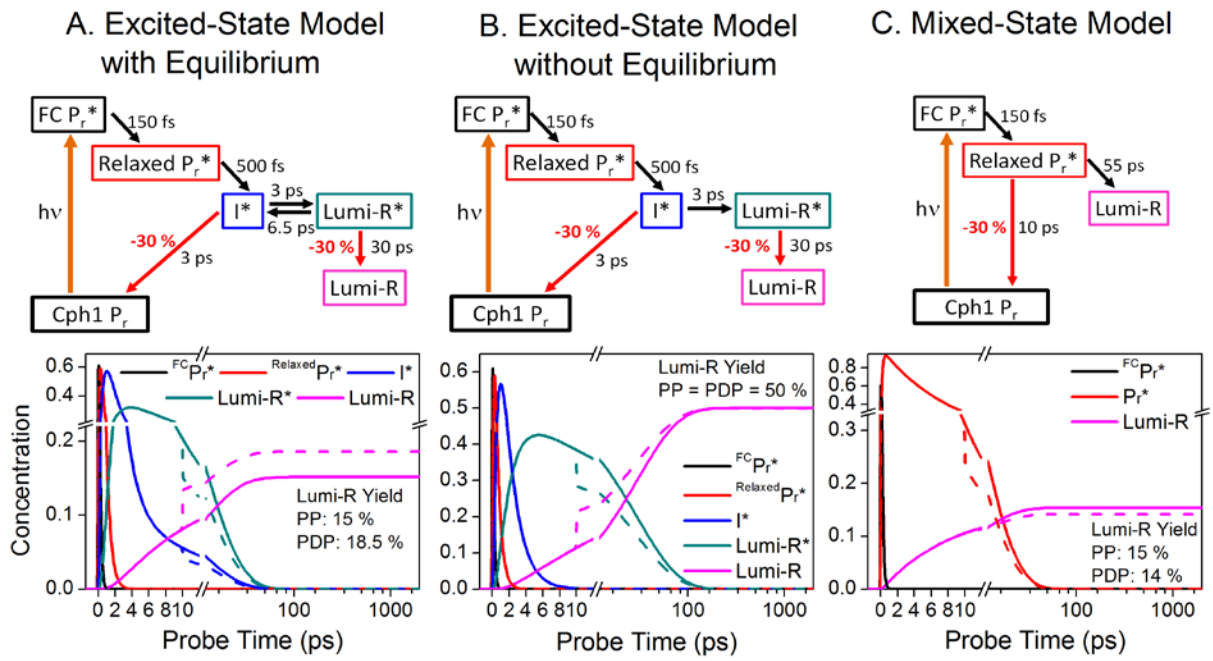

Figure S1. Simulations of three different isomerization models to interpret the dump-induced effects on the Lumi-R quantum yield. The dump efficiency was set at 30 % for all simulations, and the dumped pathway is indicated by red arrows. The top panel is the models with respective connectivity scheme and time constants and the bottom panel is the corresponding concentration profiles for the models immediately above. Spectral species are color-coded respective each other. (A) The kinetic model suggested by Dasgupta et al.[14] The 6.5 ps time constant from Lumi-R* to I* (dark cyan to blue box) is estimated to adjust the $\Phi_{pr} \approx 15$ %, suggested by previous studies.[15] (B) The model based on Panel A *without* the excited-state equilibrium, I* ⇄ Lumi-R*, which produces Lumi-R quantum yield of 50 %. (C) The simplified mixed-state model simulation, which corresponds to Figure 1C from the manuscript.

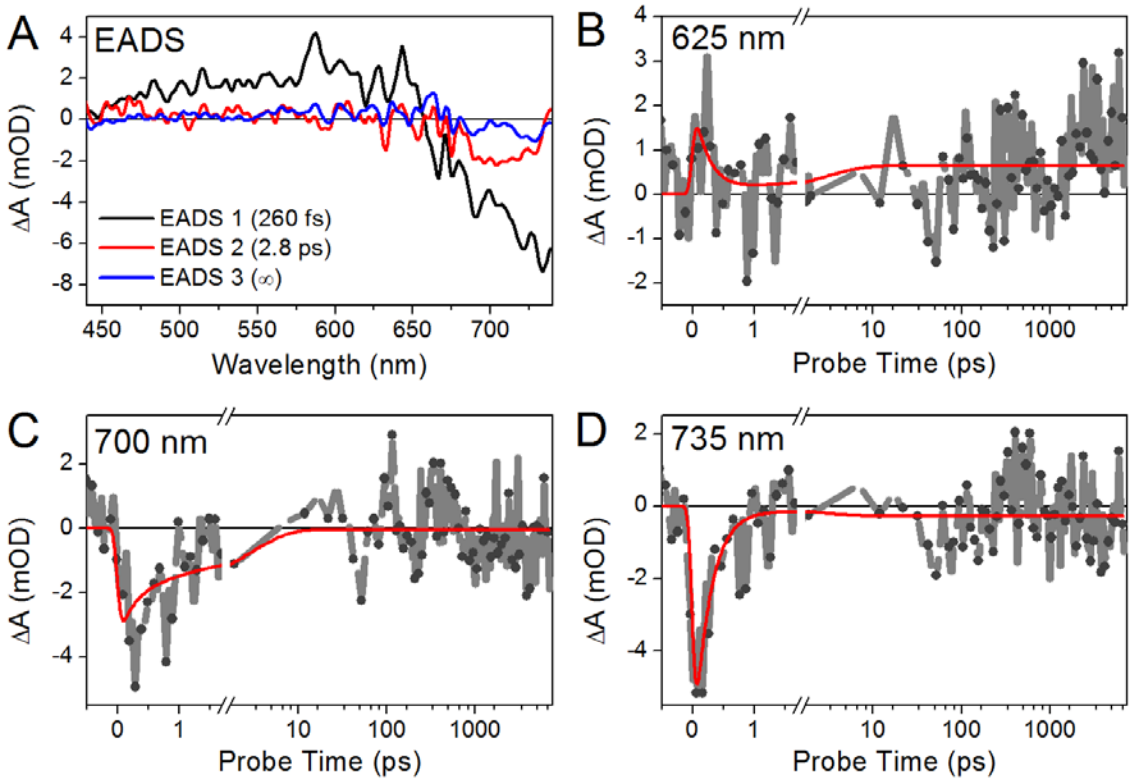

Figure S2. Dump-probe signals from the 10-ps dump PDP dataset. These signals correspond to the Cph1 reverse reaction, $P_{fr} \rightarrow P_r$, as shown by our recent characterization of that reaction.[4] (A) EADS from three-component sequential model for dump-probe signals. The time constants are identical to recently reported reverse dynamics,[4] and each EADS has comparable spectral shapes. (B, C, D) Kinetic traces of dump-probe signals at 625, 700, and 735 nm, respectively. Notice that most signals have sub-picosecond dynamics, with a small terminal amplitude.

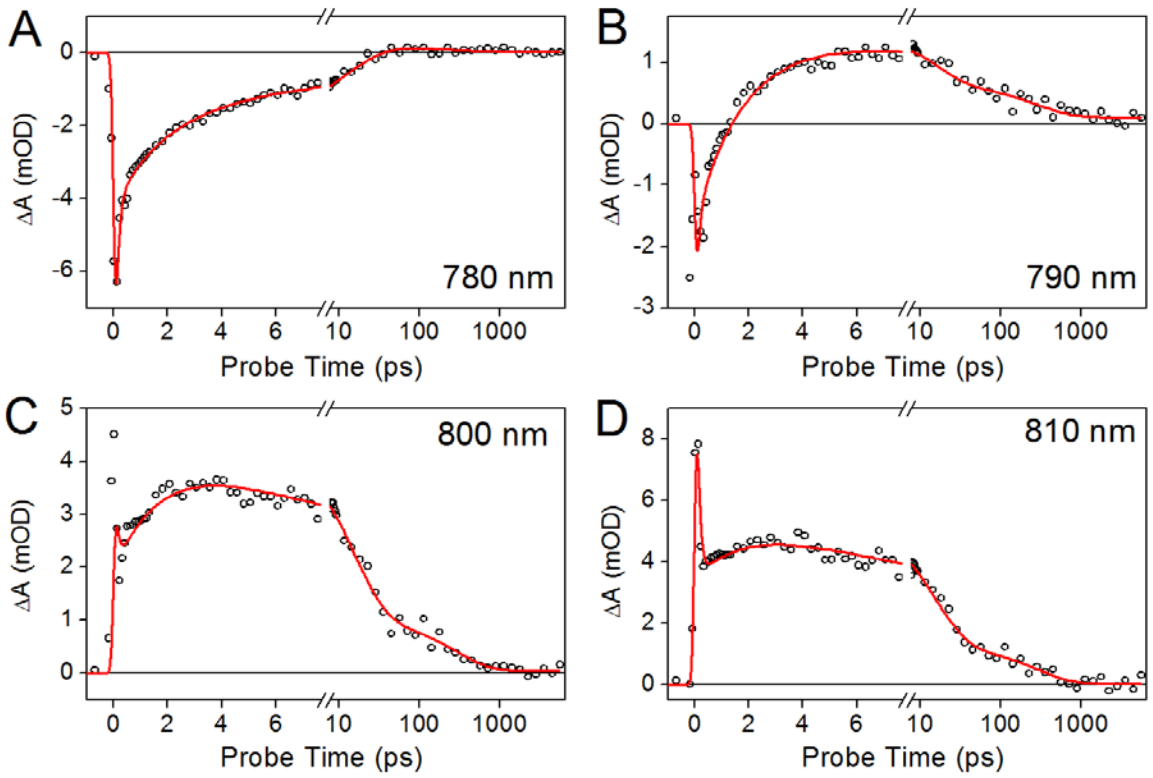

Figure S3: Kinetic traces of pump-probe data in the near-IR region from 760 to 820 nm. Traces at selected wavelengths are shown here. The red curves are the fit from the four-component global sequential model in Figure S4.

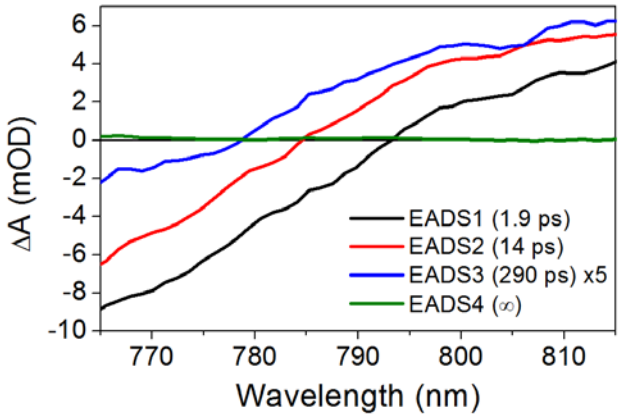

Figure S4. The Evolution Associated Difference Spectra (EADS) generated by sequential analysis of pump-probe signals in the near-Infrared region (from 760 to 820 nm). EADS3 was magnified to 500 % for better comparison with EADS1 and EADS2.

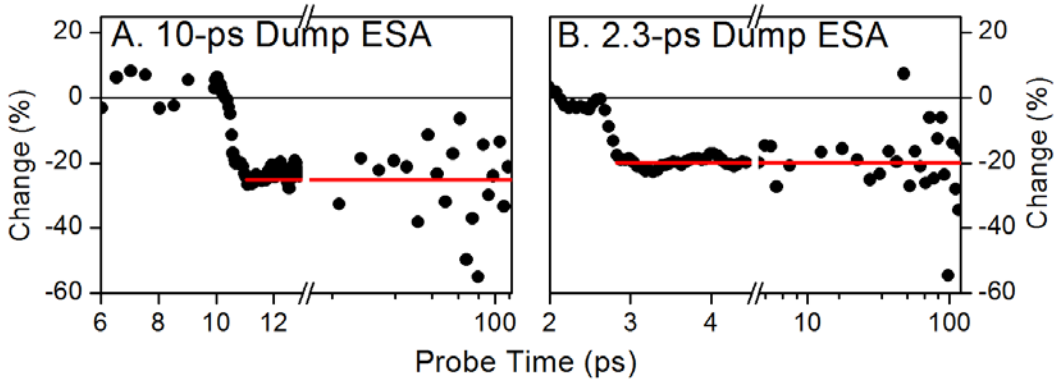

Figure S5. The relative depletion dynamics (ΔΔOD/PP x 100 %) of the ESA band in time (up to 120 ps probe time) for 10-ps (A) and 2.3-ps (B) dump pulse data sets. Depletion was averaged over the 440 to 500 nm ESA band. The horizontal red lines are the average % change from 11 to 120 ps (A) and 2.8 ps to 120 ps (B) at -25 % and -20 %, respectively.

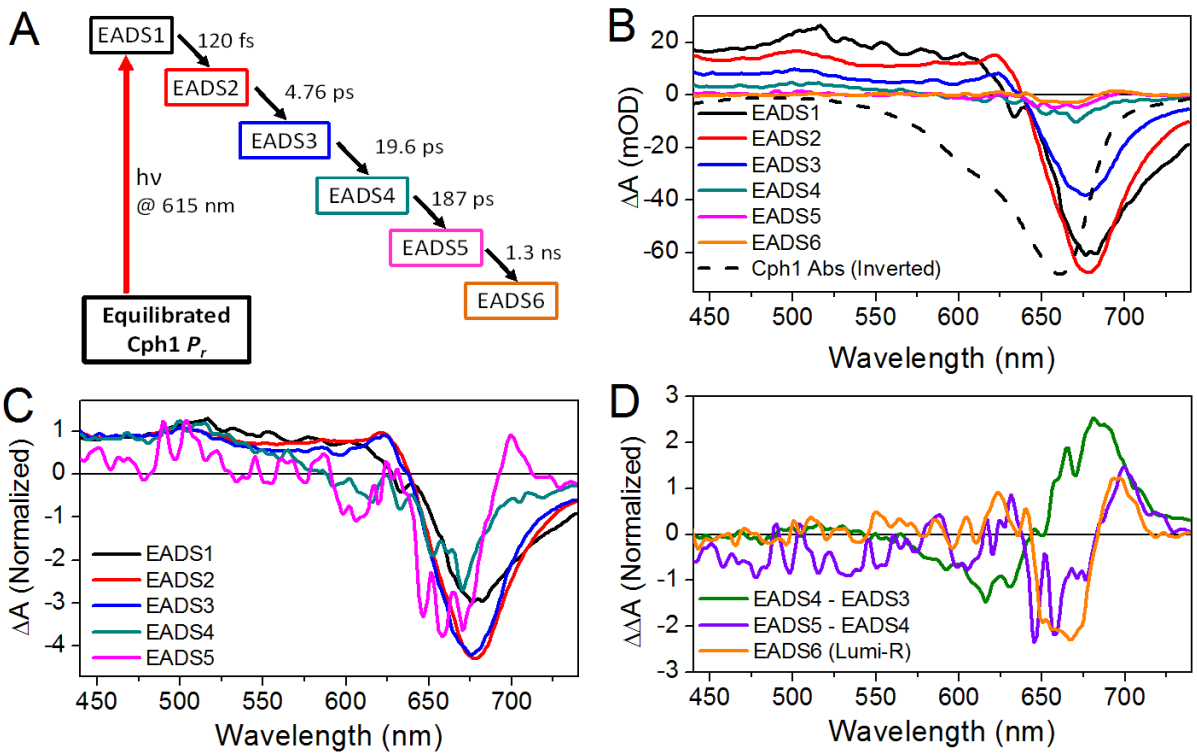

Figure S6. Sequential analysis of the 10-ps PDP datasets using a six-component model. (A) Schematic of the sequential model with corresponding decay time constants. Throughout the figure, each EADS is color-coded as in Panel A. (B) EADS from this model overlaid with the inverted P_r ground-state absorption band. (C) EADS normalized at the ESA band (440 to 500 nm). (D) Difference of subsequent EADSs was calculated to extract spectral evolution independent from excited-state decay. EADS4 – EADS3 (green) and EADS5 – EADS4 (purple) are compared with the PP EADS6 signal, which corresponds to Lumi-R photoproduct (orange curve).

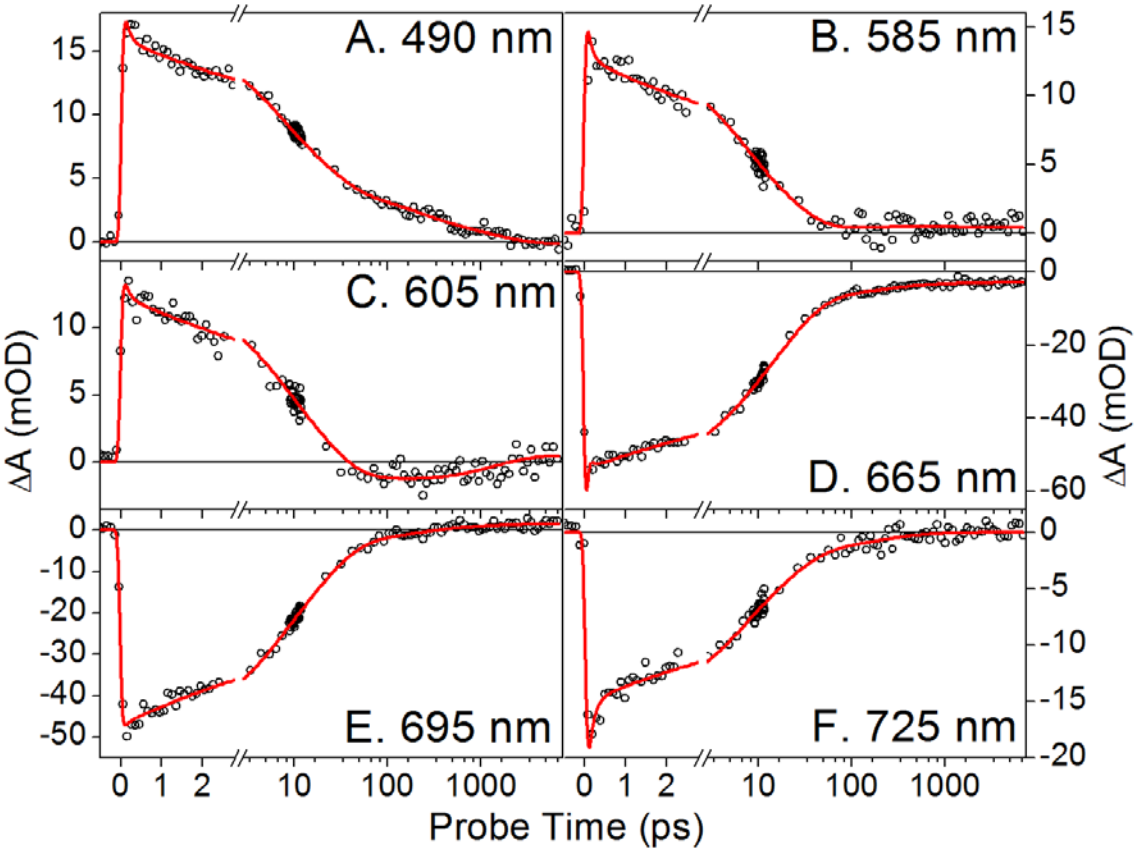

Figure S7: Kinetic traces of pump-probe data at selected wavelengths are shown fitted to the six-component sequential analysis in Figure S6A.

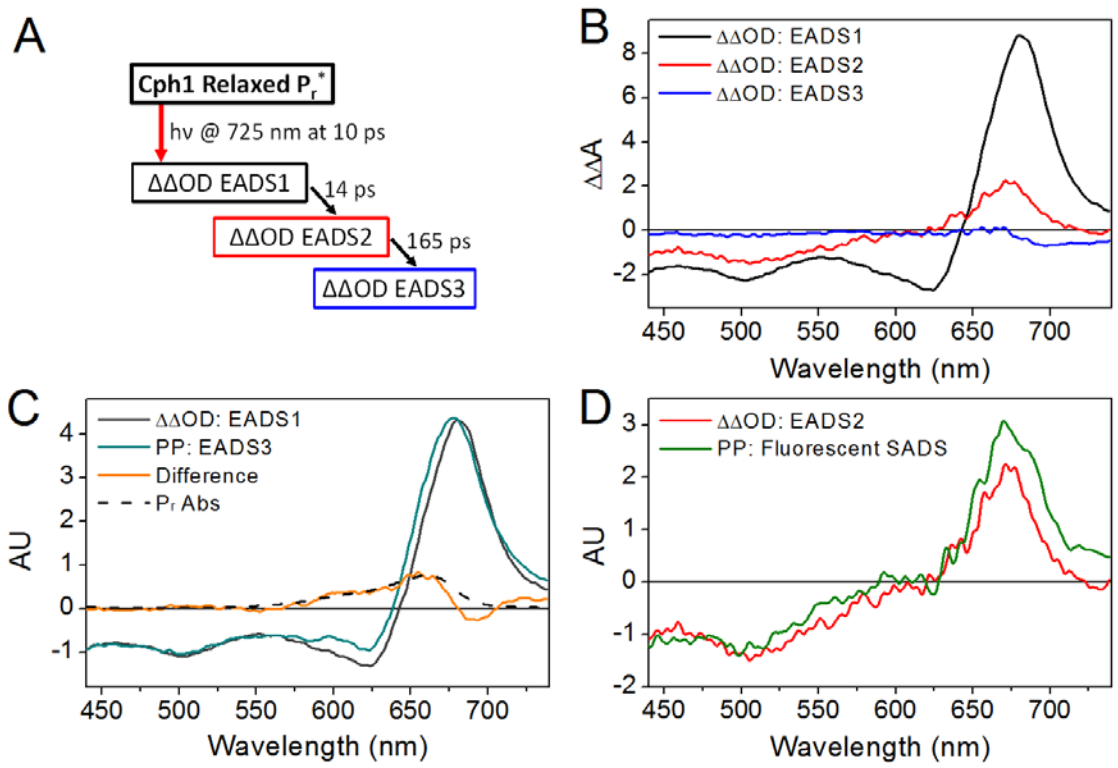

Figure S8. Sequential analysis of ΔΔOD signals from the 10-ps PDP dataset. (A) The scheme of the 3-component sequential model, with decay time constants for each EADS. (B) The EADS are plotted and color-coded to the scheme. (C) ΔΔOD EADS1 (black curve) compared with inverted PP EADS3 (dark cyan curve) from Figure S6B. The difference between them (orange curve) is also plotted and is compared with P_r absorbance. (D) ΔΔOD EADS2 (red curve) compared with inverted SADS of fluorescent populations extracted from the integrated model (Figure S12B).

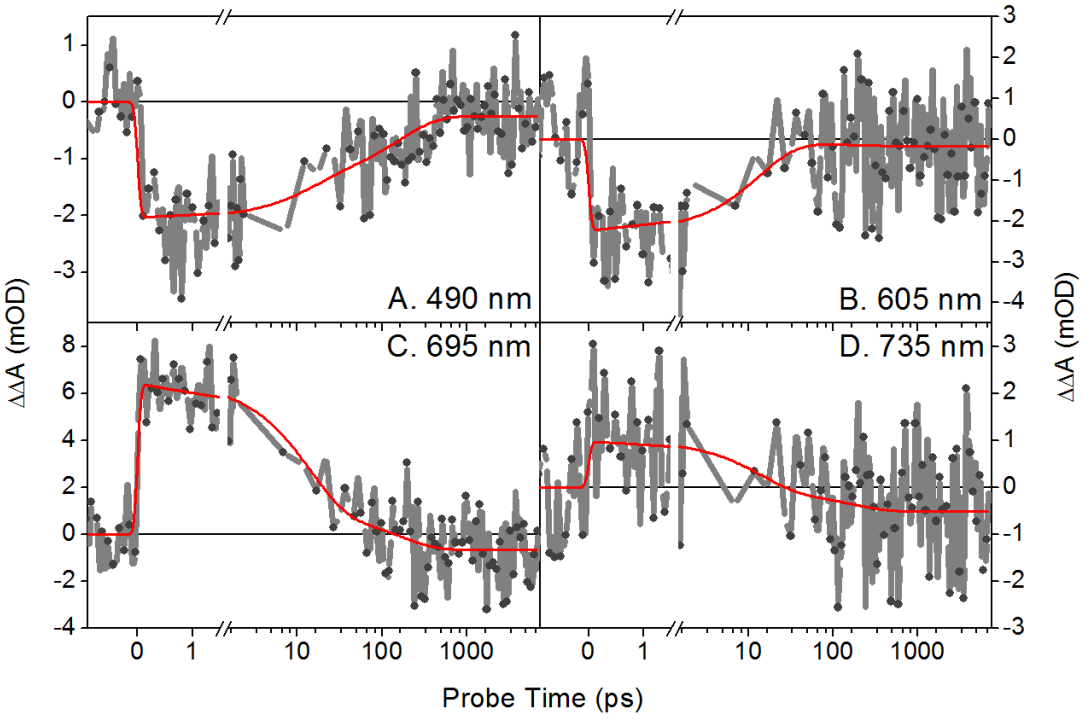

Figure S9. ΔΔOD signals from 10-ps PDP data. The x-axis is adjusted by -10 ps, such that the dump pulse is applied at apparent time zero. The red curves are calculated using the three-component sequential model in Figure S8A. This signal is clearly different from the dump-probe signals presented in Figure S2, which exhibit sub-picosecond decay and arise from the Cph1 reverse reaction.

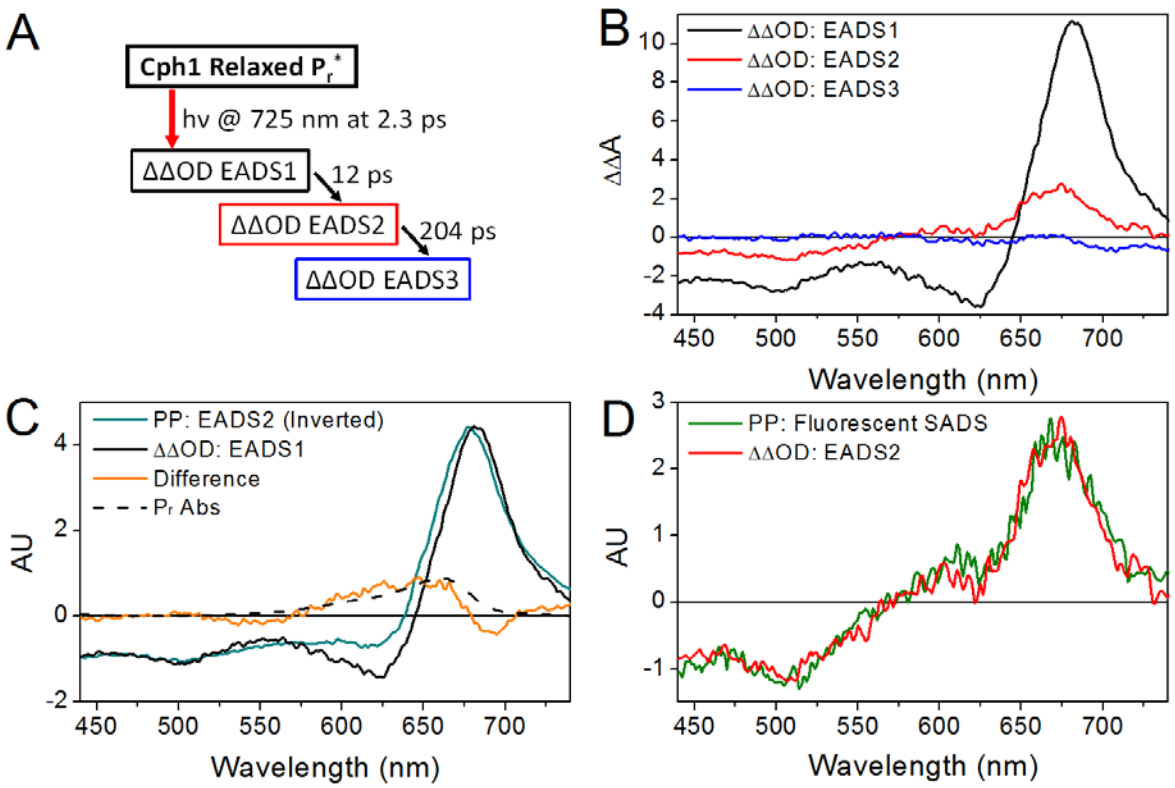

Figure S10. Sequential analysis of ΔΔOD signals from the 2.3-ps PDP dataset. (A) The scheme of the 3-component sequential model, with decay time constants for each EADS. (B) The EADS are plotted and color-coded to the scheme. (C) ΔΔOD EADS1 (black curve) compared with inverted PP EADS2 (dark cyan curve) from Figure S6B. The difference between them (orange curve) is also plotted and is compared with P_r absorbance. (D) ΔΔOD EADS2 (red curve) compared with inverted SADS of fluorescent populations extracted from the integrated model (Figure S14B).

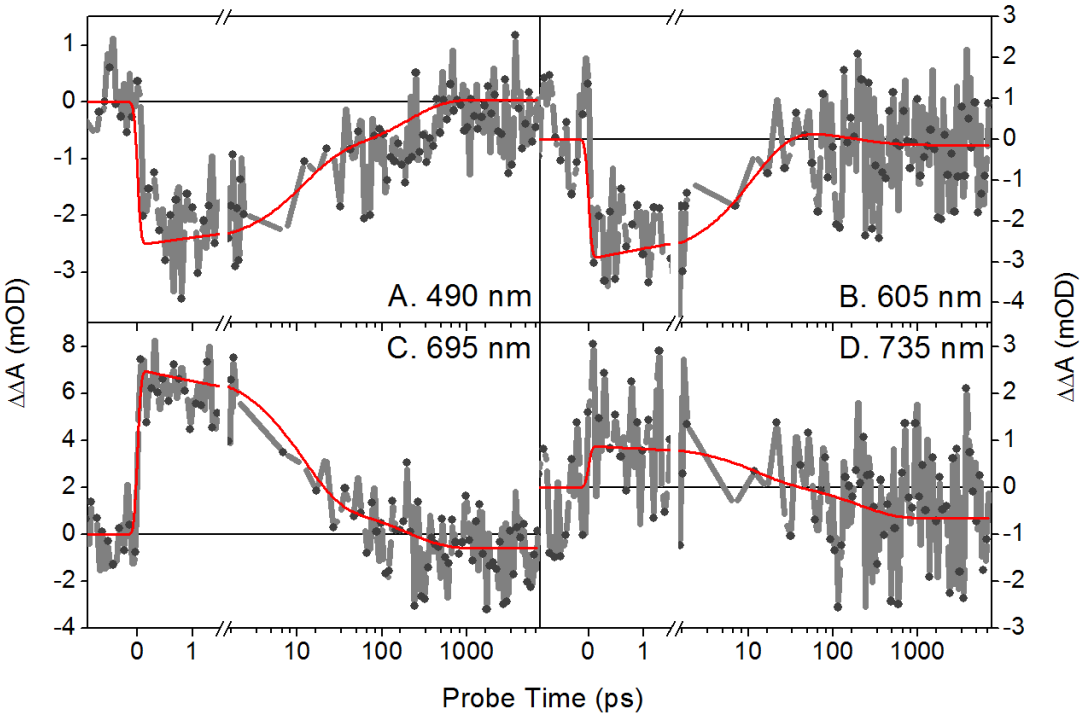

Figure S11. ΔΔOD kinetic traces from the 2.3-ps PDP data. The time axis is shifted by -2.3 ps, such that the dump pulse is applied at the apparent time zero. The red curves are calculated using the three-component sequential model in Figure S10A. This signal is distinctly different from Cph1 reverse dynamics observed in the dump-probe signals presented in Figure S2.

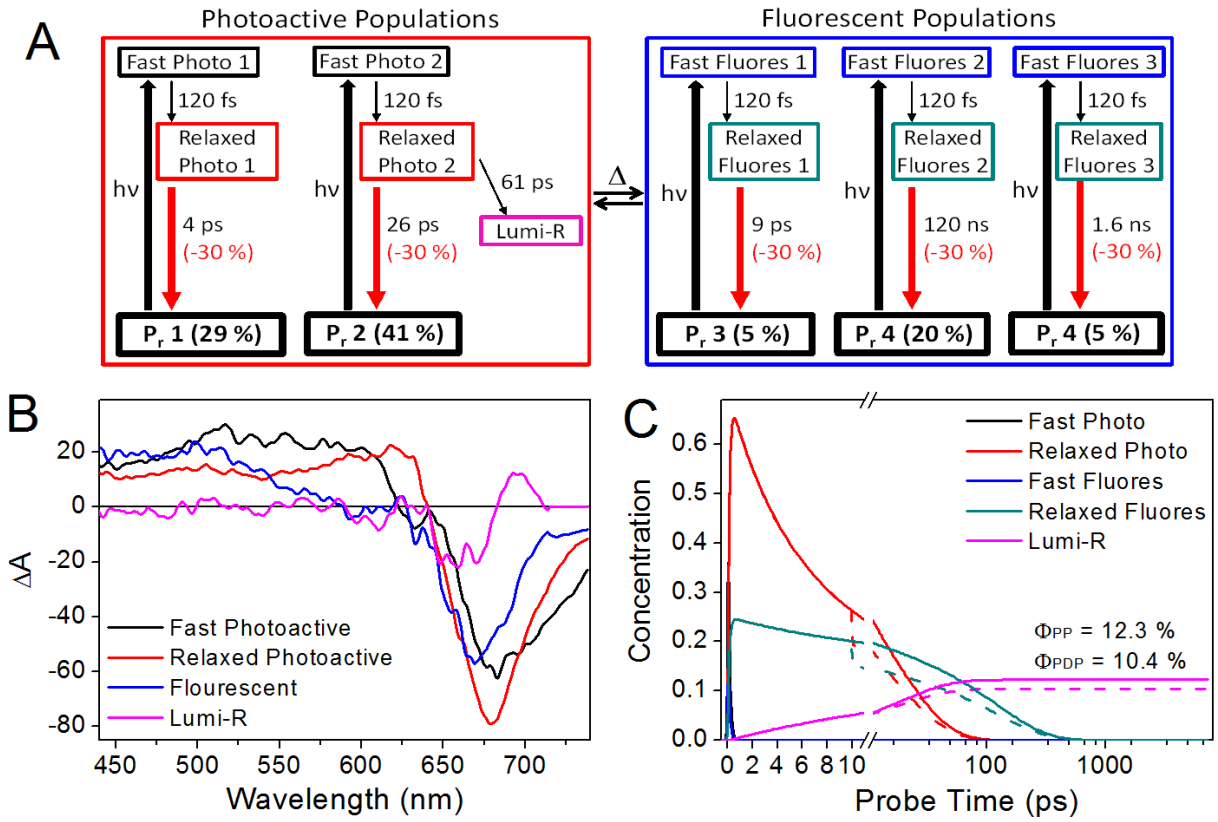

Figure S12. Global target analysis of 10-ps PDP data. (A) Integrated kinetic model with five ground-state components P_r 1 to 5. Occupancy percent of initially excited populations is indicated in parenthesis. P_r 1 and 2 belong to photoactive populations and P_r 3 to 5 belong to fluorescent populations. Red arrows indicate dump depletion path, and this model estimated dump efficiency of the experiment to be -30 %. All spectral states are color-coded in this figure. (B) Species-associated-difference-spectra (SADS). (C) Concentration profile of each spectral type, i.e., Fast Photo (Fast Photo 1 + Fast Photo 2) and Fast Fluores (Fast Fluores 1 + Fast Fluores 2 + Fast Fluores 3) based on the target model in Panel A. The solid lines are the PP signals and the dashed lines are the PDP signals. The final Lumi-R population shows dump-induced depletion from PP signals of 12.3 % to 10.4 %.

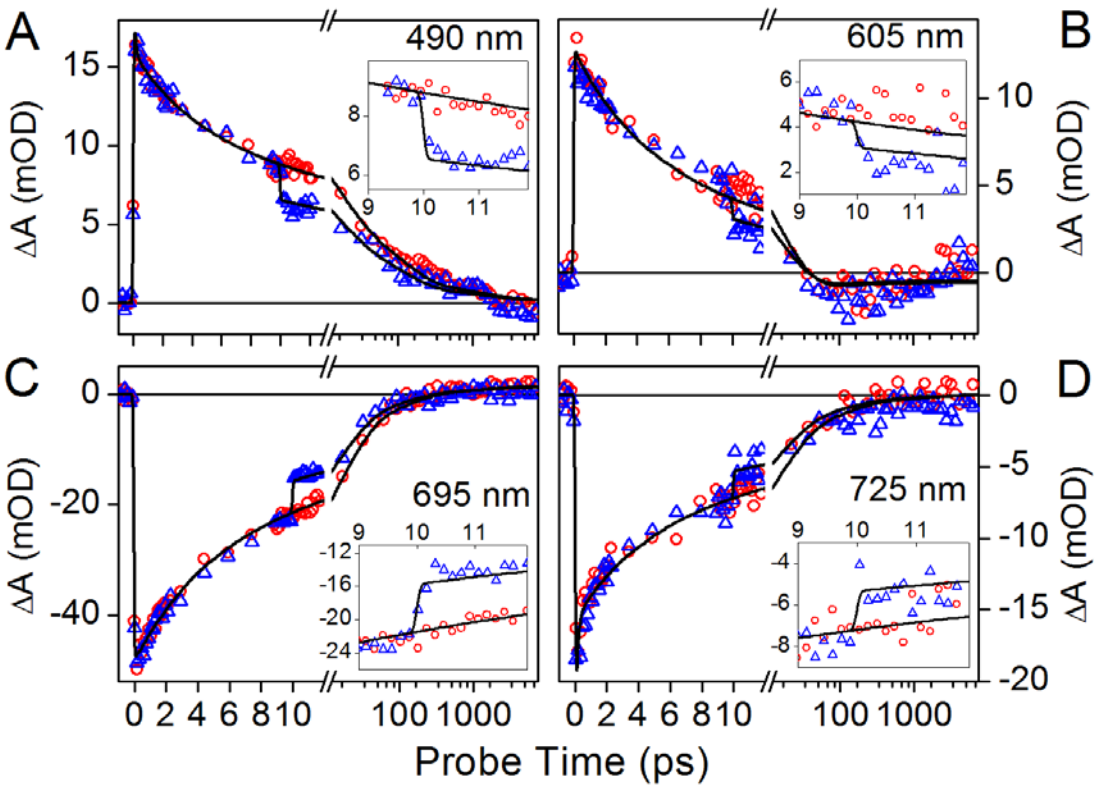

Figure S13. PP (red circles) and PDP (blue triangles) kinetic traces of 10-ps PDP data are shown for selected wavelengths. Data are globally fit (black curves) to the target model presented in Figure S12A. Insets emphasize data and fitting right before and after application of the 10-ps dump pulse.

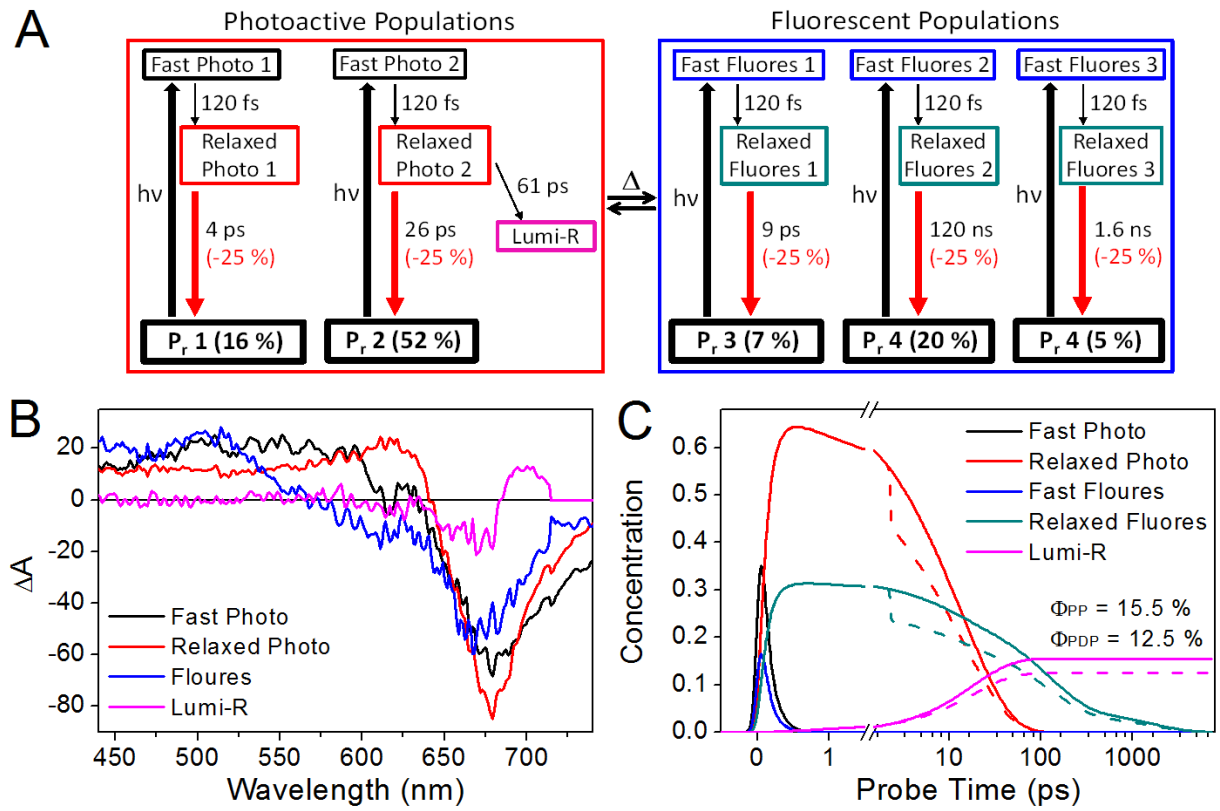

Figure S14. Global target analysis of the 2.3-ps PDP data. (A) Integrated kinetic model with five ground-state components P_r 1 to 5. Occupancy percent of initially excited populations is indicated in parenthesis. P_r 1 and 2 belong to photoactive populations and P_r 3 to 5 belong to fluorescent populations. This occupancy is different from that of 10-ps PDP signals (Figure S12A), indicating sample-to-sample variation in heterogeneous thermal equilibrium. Red arrows indicate dump depletion path, and this model estimated dump efficiency of the experiment to be -25 % in compared to -30 % of 10-ps PDP signals (Figure S12A). All spectral states are color-coded in this figure. (B) Species-associated-difference-spectra (SADS). (C) Concentration profile of each spectral type, i.e., Fast Photo (Fast Photo 1 + Fast Photo 2) and Fast Fluores (Fast Fluores 1 + Fast Fluores 2 + Fast Fluores 3) based on the target model in Panel A. The solid lines are the PP signals and the dashed lines are the PDP signals. The final Lumi-R population shows dump-induced depletion from PP signals of 15.5 % to 12.5 %.

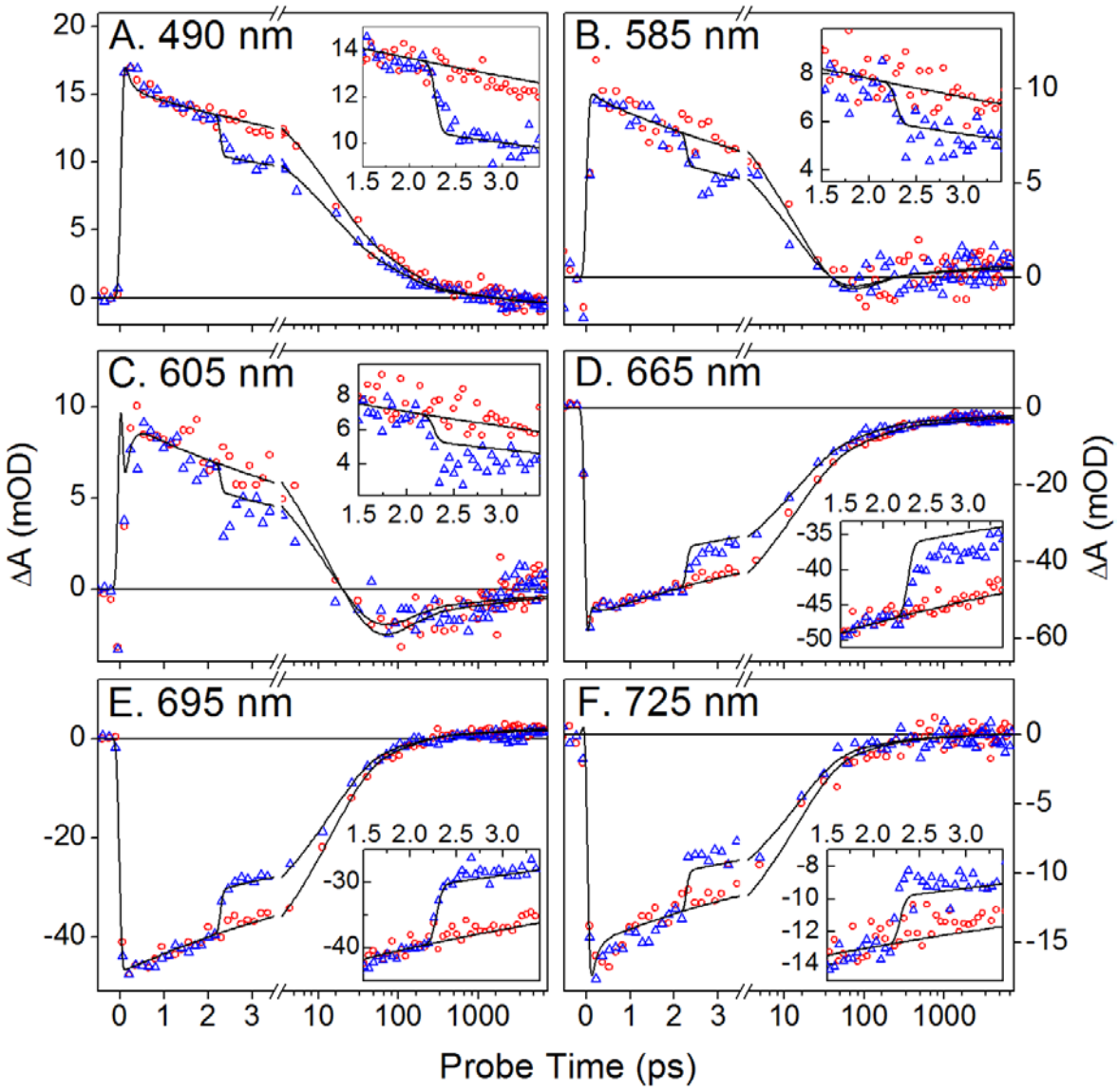

Figure S15. PP (red circles) and PDP (blue triangles) kinetic traces from the 2.3-ps PDP dataset are presented for selected wavelengths. Traces were fitted to the target model in Figure S14A. Insets emphasize data and fitting right before and after application of the 2.3-ps dump pulse.

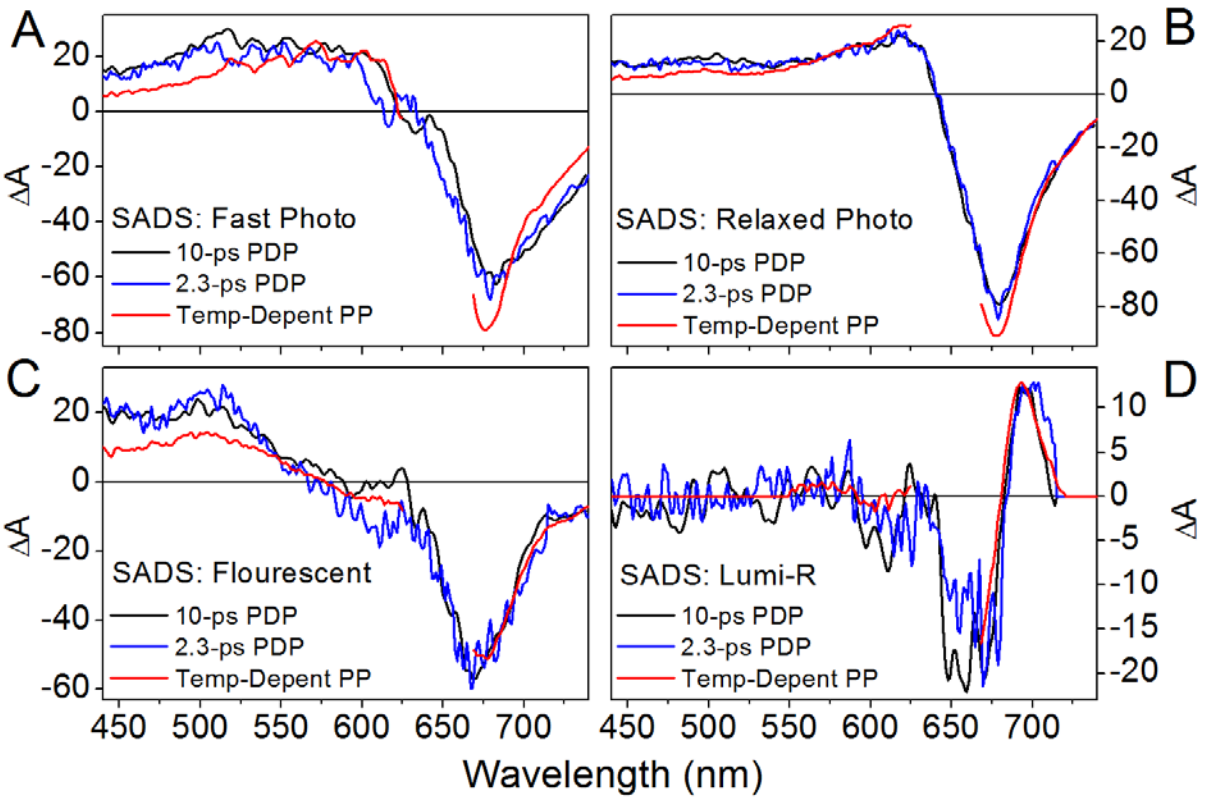

Figure S16. Comparison of integrated model SADS from 10-ps and 2.3-ps PDP signals (black and blue curves, respectively) and temperature-dependent PP study at 25 °C (red curves)[8] for (A) Fast Photoactive, (B) Relaxed Photoactive, (C) Fluorescent and (D) Lumi-R populations. The SADS from the temperature-dependent PP study are uniformly scaled (× 11) to compare with PDP signals.

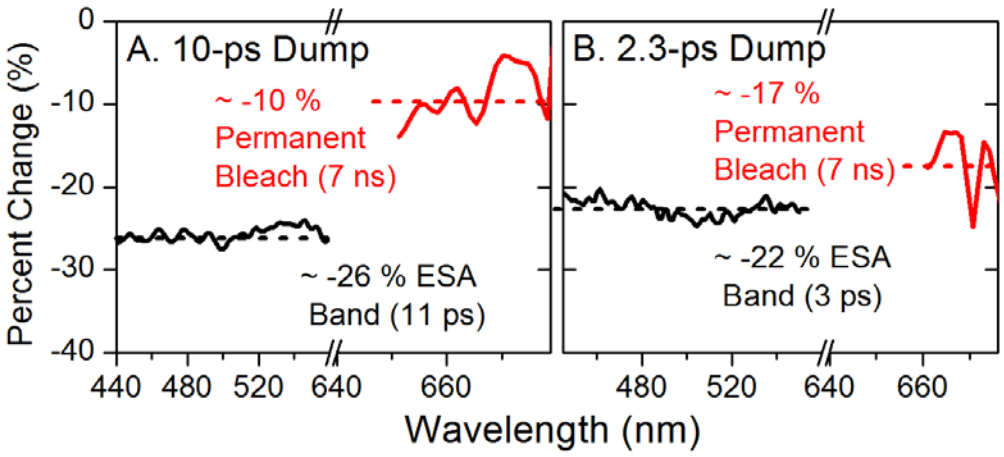

Figure S17. Relative Lumi-R depletion upon dumping (ΔΔOD/PP x 100 %) was measured using high-average data collection at a single probe time (7 ns). (A) Comparison between 10-ps dump-induced initial excited-state depletion at 11 ps (black curve, ESA band) and final Lumi-R yield depletion (red curve, permanent P_r bleach band). Lumi-R formation is reduced by the dump pulse. Quantitatively, Lumi-R depletion (-10 %) is 38% of the initial excited-state depletion (-26 %). (B) Comparison between 2.3-ps dump-induced initial excited-state depletion at 3 ps (black curve) and Lumi-R depletion (red curve). Lumi-R depletion (-17 %) is 78% of the initial excited-state depletion (-22 %). Dashed lines are the average bleach values. From the mixed state model (Figure S12).